The ARH and Macrodomain Families of α-ADP-ribose-acceptor Hydrolases Catalyze α-NAD^+ Hydrolysis.

Linda A. Stevens[1], Jiro Kato[1], Atsushi Kasamatsu[1,3], Hirotake Oda[1], Duck-Yeon Lee[2] and Joel Moss[1*].

[1]Pulmonary Branch and [2] Biochemistry Core facility, National Heart, Lung, and Blood Institute, National Institutes of Health, Bethesda, MD 20892-1590, USA

Present address:[3]Department of Oral Science, Graduate School of Medicine, Chiba University 1-8-1 Inohana, Chuo-ku, Chiba 260-8670, Japan

*Correspondence: mossj@nhlbi.nih.gov

Figure S1

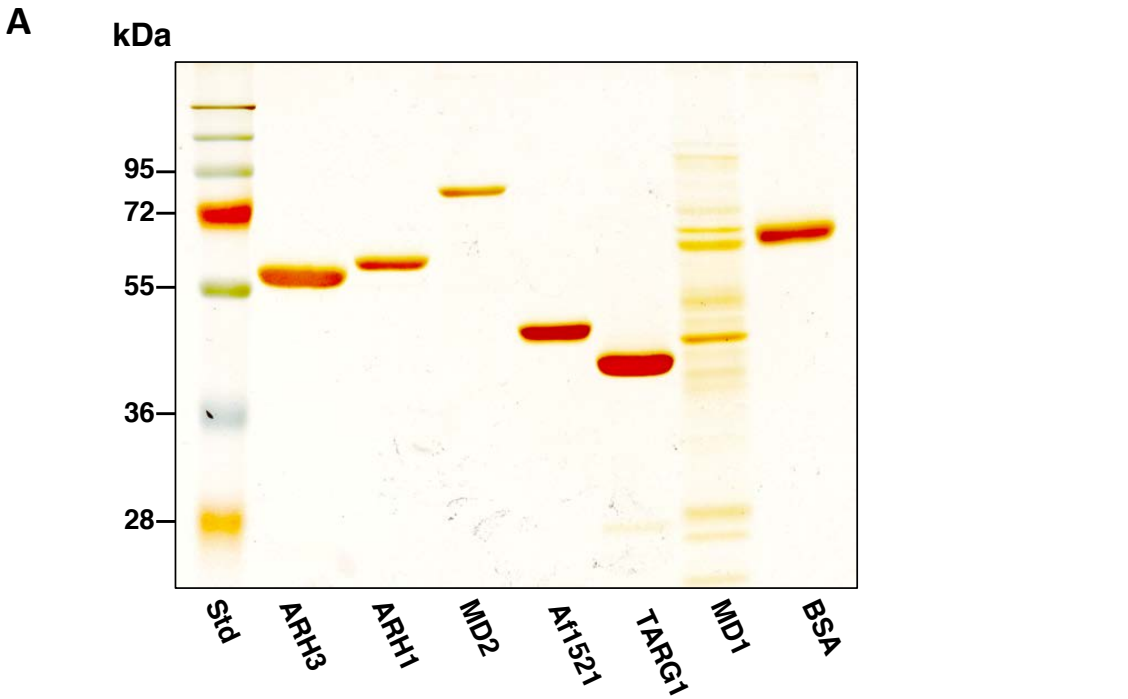

Silver Stain gel, 3ug purified

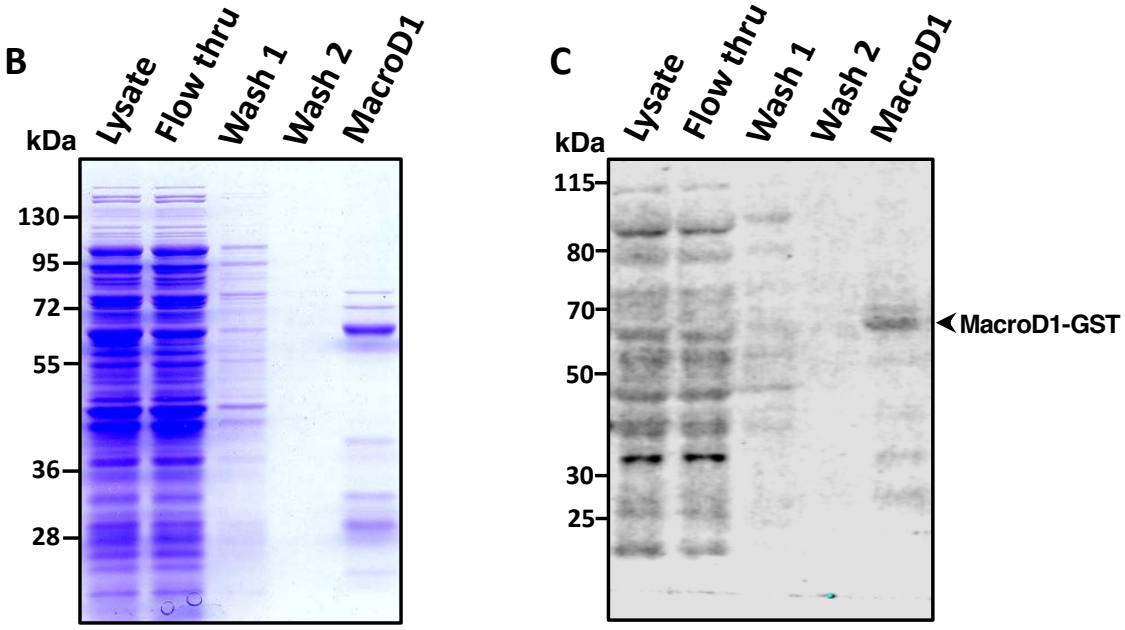

Figure S1. Separation of purified Macrodomains and ARHs by SDS-PAGE.
A. To determine the purity of the protein preparations, 3µg of purified ARH1, ARH3, TARG1, MacroD1, MacroD2 and Af1521 and molecular weight protein ladder (Crystalgen) were separated by SDS-PAGE using 12% gels, which were incubated with silver stain (Thermo Scientific). BSA (3µg) was included as a molecular weight marker. B,C. MacroD1 was expressed in *E.coli* with 6xhis/GST tag (see Methods). Recombinant protein was purified by Ni-NTA affinity column (QIAexpress Ni-NTA Fast Start, Qiagen). Lysate (5µl), flow through (5µl) and purified protein (5µl, 3.4µg) were separation on SDS PAGE (10% gel), stained with Coomassie blue (B) and immunoreacted with Anti-Mouse-GST tag monoclonal antibody (Invitrogen) (C).

Figure S2

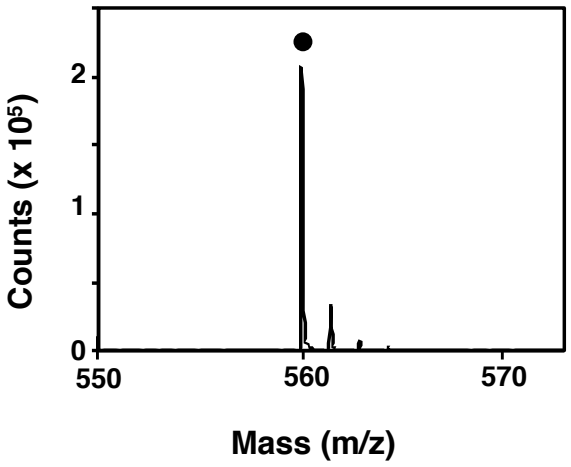

Figure S2. Mass spectral analysis of α-NADase reaction product.

Identity of the reaction product in the reaction mixtures was determined by isolation of the reaction products following incubation of ARH3 and α-NAD^+. The reaction mix was separated on an HPLC Discovery Bio Wide Pore C18 column (Supelco) equilibrated with water containing 0.05%TFA for 15 min, followed by a gradient to 100% acetonitrile 0.05% TFA from 15 to 20 minutes. The peak from the reaction separation that co-eluted with pure ADP-ribose was collected and analyzed by MS and confirmed to be ADP-ribose, theoretical mass=560.080.

Figure S3

A

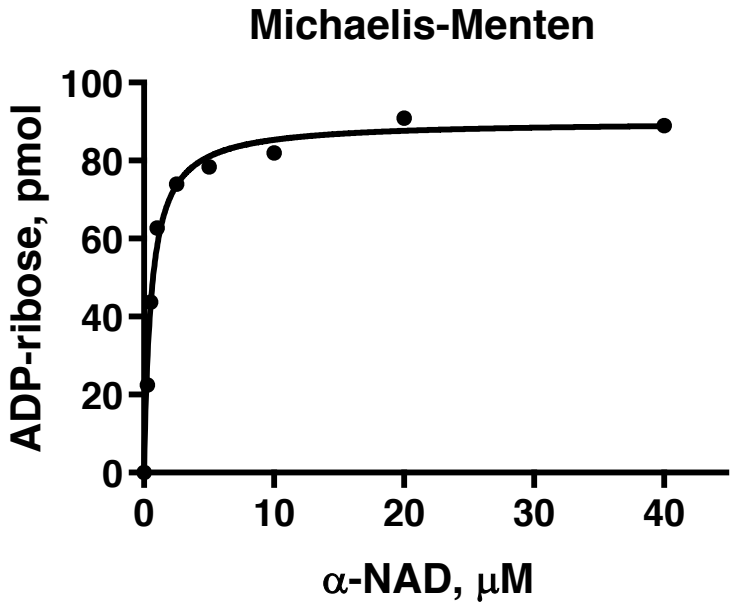

B

Michaelis-Menten	ADP-Ribose, pmol
Best-fit values	
Vmax	90.08
Km	0.5582
Std. Error	
Vmax	1.977
Km	0.06227
95% CI (asymptotic)	
Vmax	85.4 to 94.75
Km	0.4109 to 0.7054
Goodness of Fit	
Degrees of Freedom	7
R square	0.9897
Absolute Sum of Squares	83.17
Sy.x	3.447
Constraints	
Km	Km > 0
Number of points	
# of X values	27
# Y values analyzed	9

Figure S3. Kinetic Measurement of α-NAD^+ hydrolysis reaction by ARH.
A. Michaelis-Menten kinetics plot shows the enzymatic reaction of α-NADase activity by recombinant human ARH3. B. Data in table show Vmax and Km including 95% confidence interval (CI) generated by GraphPad Prism, version 8. The α-NADase activity of Af1521, ARH1, TARG1, MacroD1 and MacroD2 is too low to accurately determine the α-NAD^+ Km and Vmax.

Figure S4

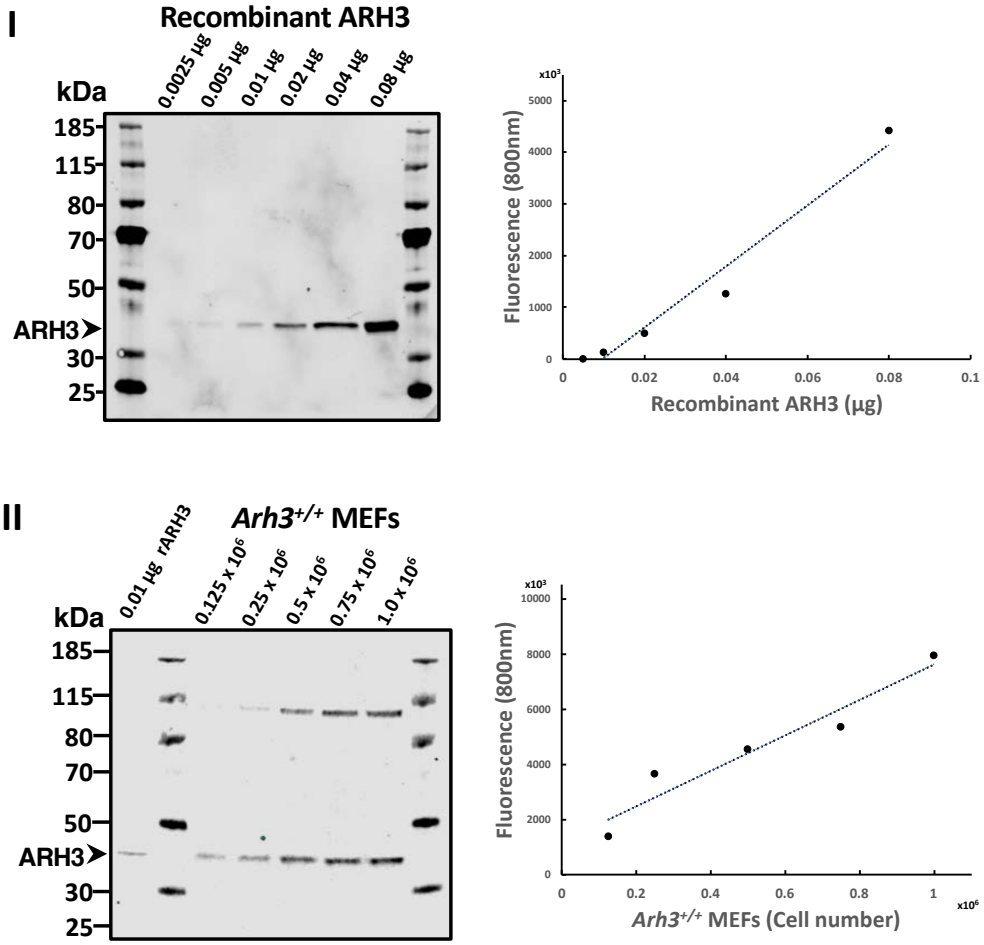
I
Recombinant ARH3
0.0025 µg
0.005 µg
0.01 µg
0.02 µg
0.04 µg
0.08 µg
kDa
185
115
80
70
50
ARH3
30
25
x10³
5000
4000
3000
2000
1000
0
Fluorescence (800nm)
0
0.02
0.04
0.06
0.08
0.1
Recombinant ARH3 (µg)
II
Arh3+/+ MEFs
0.01 µg rARH3
0.125 x 10⁶
0.25 x 10⁶
0.5 x 10⁶
0.75 x 10⁶
1.0 x 10⁶
kDa
185
115
80
70
50
ARH3
30
25
x10³
10000
8000
6000
4000
2000
0
Fluorescence (800nm)
0
0.2
0.4
0.6
0.8
1
x10⁶
Arh3+/+ MEFs (Cell number)

Figure S4. The copy number of ARH3 protein.
The Western blot analysis for recombinant ARH3 (**I**, 0.0025-0.08μg) and WT *Arh3*$^{+/+}$ MEF cell lysates (**II,** 0.125x10^6-1.0x10^6 cells) were incubated with fluorescence-labeled secondary antibody to quantify the bands for detection using the Odyssey infrared Imaging System and repeated twice. The copy number of ARH3 protein was calculated by the approximate straight lines of recombinant ARH3 and WT *Arh3*$^{+/+}$ MEF lysates.

The total protein in 1 x 10^6 MEFs was 280μg and the total ARH3 is 0.172 x 10^{-6} μg. The copy number of ARH3 protein was 172 x 10^{-3} pg/cell. The percentage of in WT *Arh3*$^{+/+}$ MEF cells was 0.06 %.

Figure S5

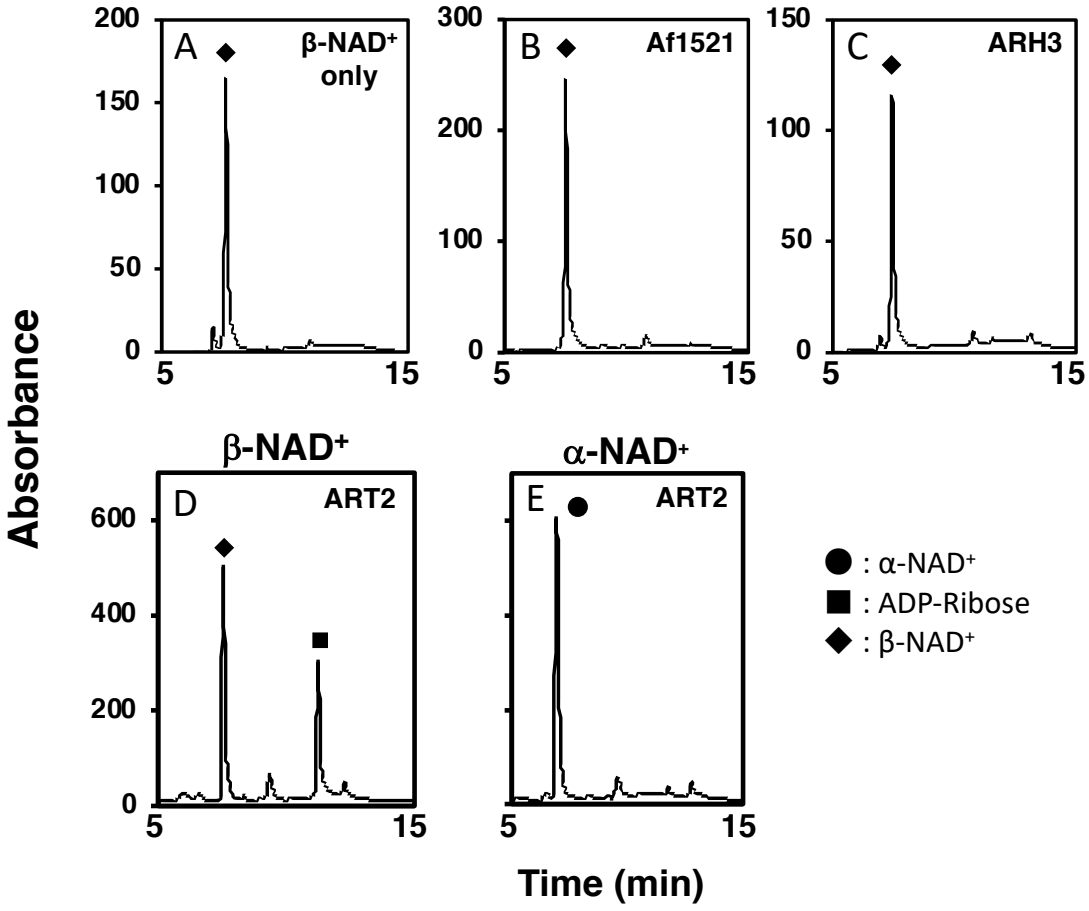
A
β-NAD+ only
B
Af1521
C
ARH3
β-NAD+
D
ART2
α-NAD+
E
ART2
Absorbance
Time (min)
● : α-NAD+
■ : ADP-Ribose
◆ : β-NAD+

Figure S5. HPLC separation of α-NADase reaction mixes containing β-NAD^+ with either Af1521, ARH3 or ART2.

ARH3 and macrodomain Af1521 were incubated with β-NAD^+ (50μM) in 50mM Tris pH 7.5, with (ARH3) or without 10mM $MgCl_2$ in 200μl of reaction mix containing **A**. (◆) β-NAD^+ (50μM) only or **B**. with Af1521 (10.2μg), or **C**. ARH3 (0.5μg) for 1hr at 37°C before 50ul of the reaction products were separated by HPLC, monitored at 258nm as described in Methods**.** ART2 (RT6.2) PIPLC supernatant (125μl) (see Methods) was incubated with 50μM α-NAD^+ (E,●)or β-NAD^+ (D, ◆)(5 assays each) in 200μl PBS reaction mix for 30°C 1hr. The reaction products (■ ADP-ribose) from 200μl of reaction mixture were separated by HPLC, monitored at 258nm as described above. Data represent a single separation.

Figure S6

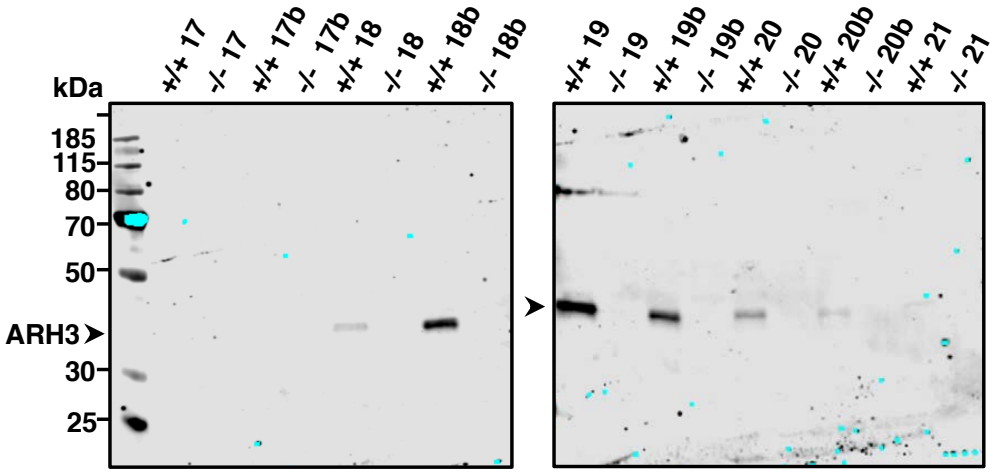
+/+ 17
-/- 17
+/+ 17b
-/- 17b
+/+ 18
-/- 18
+/+ 18b
-/- 18b
+/+ 19
-/- 19
+/+ 19b
-/- 19b
+/+ 20
-/- 20
+/+ 20b
-/- 20b
+/+ 21
-/- 21
kDa
185
115
80
70
50
ARH3
30
25

Figure S6. Immunoreactivity of ARH3 in HPLC separations of *Arh3*$^{+/+}$ WT and *Arh3* $^{-/-}$ MEF lysates.

Arh3$^{+/+}$ WT MEF (2.6 mg) and *Arh3*$^{-/-}$ MEF (2.6 mg) lysates were separated by molecular size by HPLC in a TSK-GEL (Tosohaas, G3000sw) column by PBS isocratic elution (flow=1ml/min) into 0.5ml fractions (17-21b, b=0.5min). Fractions (25µl) were separated by SDS-PAGE then analyzed for the expression of ARH3 immunoreactivity by Western blot (see Methods).

Figure S7

I : *Arh3*$^{+/+}$ MEFs

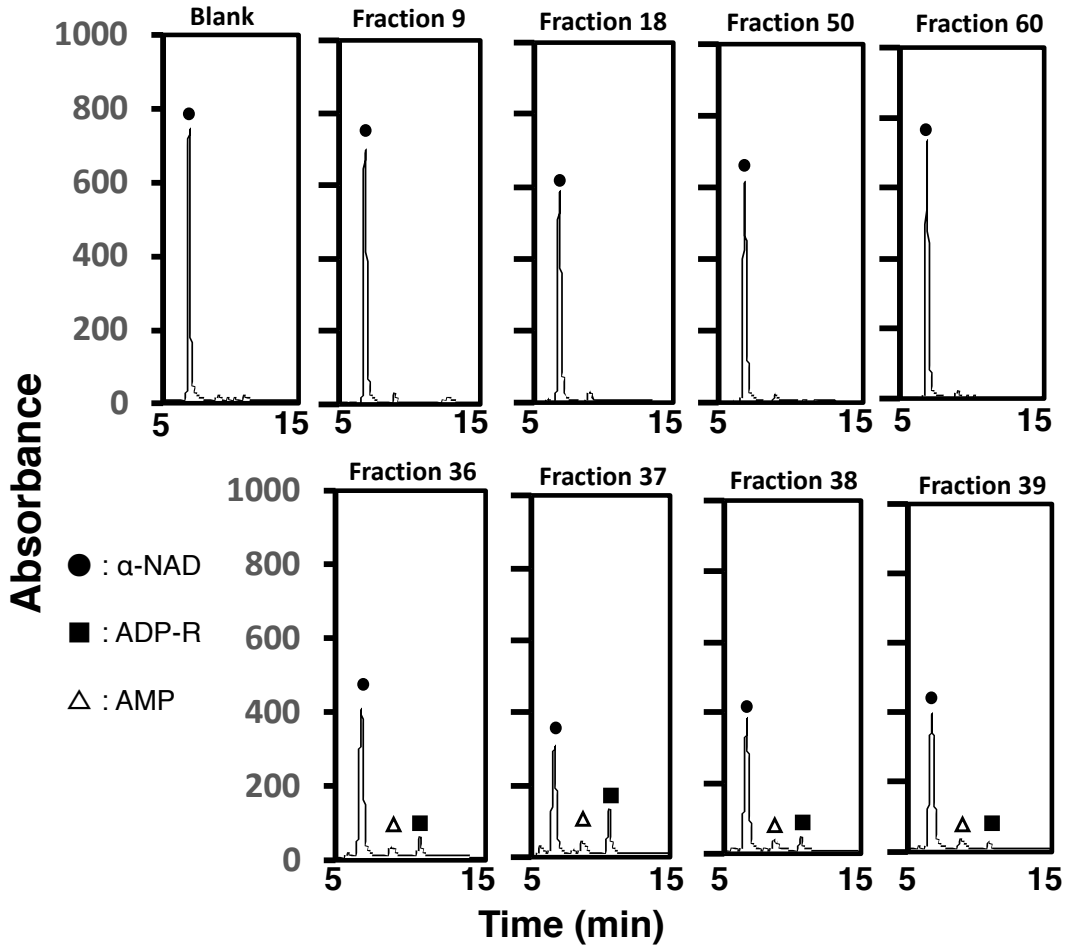

II : *Arh3*$^{-/-}$ MEFs

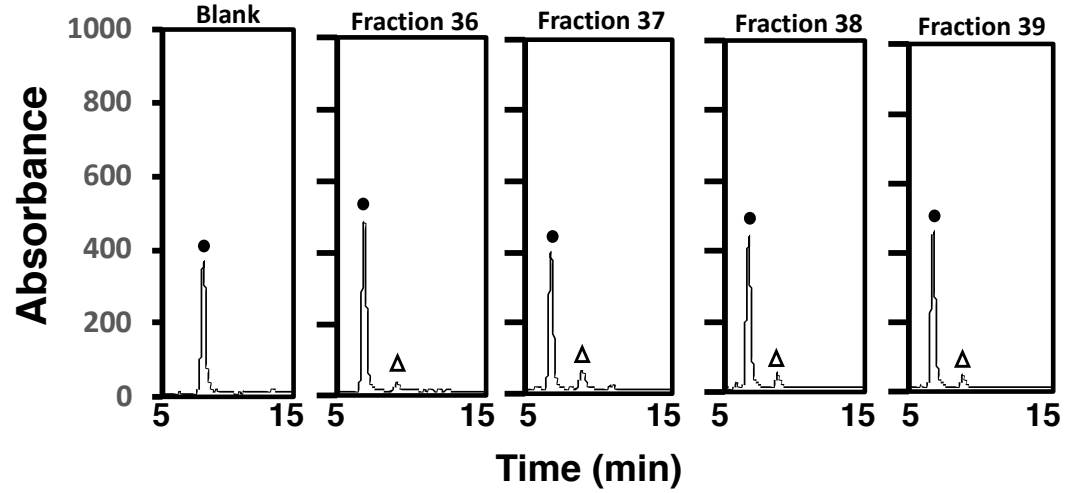

Figure S7. HPLC separation of reaction mixes from weak-anion exchange chromatography in Figure 2-II.

WT *Arh3*$^{+/+}$ and *Arh3*$^{-/-}$ MEF lysates were separated by weak-anion exchange HPLC. Fractions were incubated with α-NAD (●) and analyzed for α-NADase activity hydrolysis product, ADP-ribose (■) as described in Methods, (Figure 2-**II**). A small amount of AMP (△) was detected in some fractions. ADP-ribose was identified in fractions 36-39 from WT *Arh3*$^{+/+}$ MEF lysate (**I**). ADP-ribose was not detected in the corresponding fractions (36-39) from *Arh3*$^{-/-}$ MEF lysate (**II**) or in fractions 9,18,50,60 from WT *Arh3*$^{+/+}$ (**I**).

Figure S8

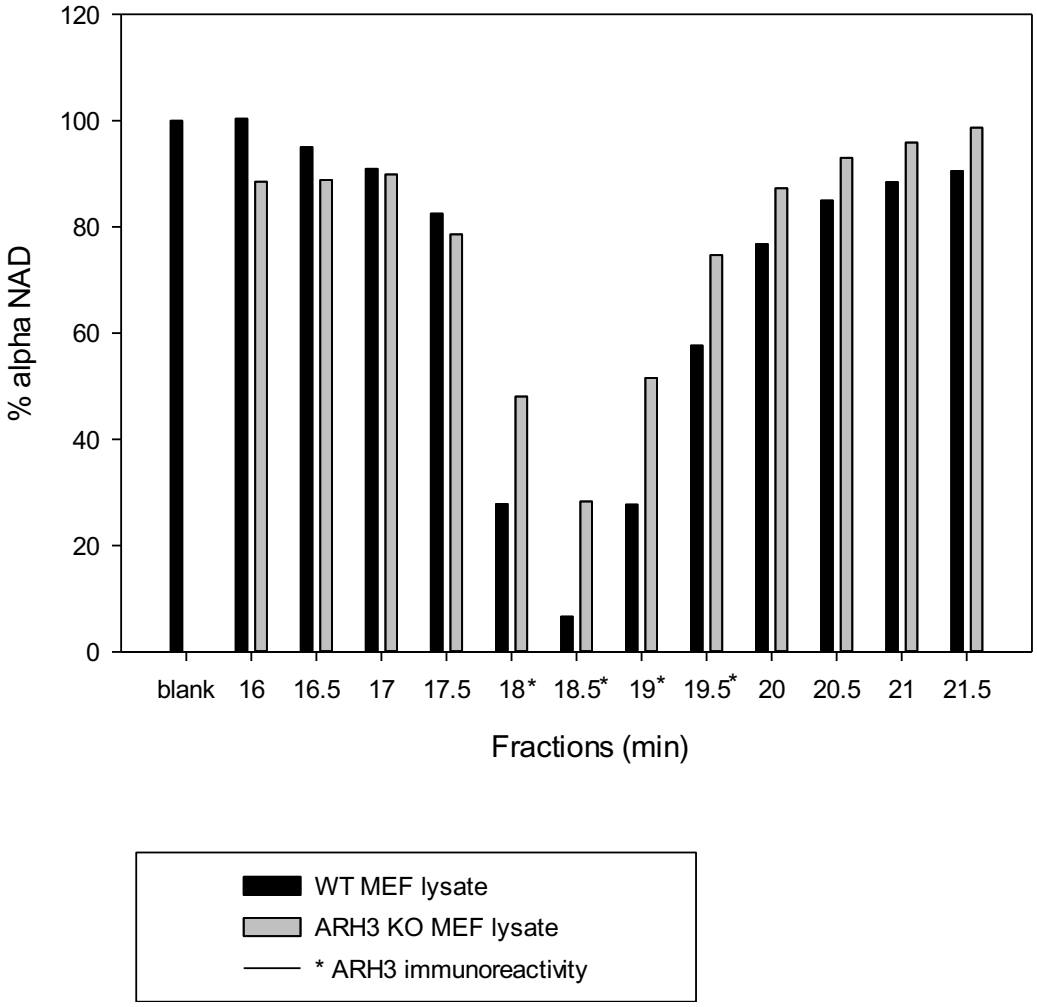
120
100
80
60
40
20
0
% alpha NAD
blank
16
16.5
17
17.5
18*
18.5*
19*
19.5*
20
20.5
21
21.5
Fractions (min)
WT MEF lysate
ARH3 KO MEF lysate
* ARH3 immunoreactivity

Figure S8. α-NAD consumption.
WT *Arh3*$^{+/+}$ MEF (2.6mg) and ARH3 KO MEFs (2.6 mg) lysates were separated by molecular size by HPLC in a TSK-GEL (Tosohaas, G3000sw) column by PBS isocratic elution into 0.5ml fractions. Fractions (200 µl) were assayed for α-NADase activity 3h at 30°C. Fractions (25µl) were analyzed for the expression of ARH3 immunoreactivity* as described in Methods. We did not observe an increase in α-NAD^{+} above background levels in the *Arh3*$^{-/-}$ MEFs.

Figure S9

A

Sample	α-NAD (Peak Abs. 258nm)	AMP (Peak Abs. 258nm)	ADPr (Peak Abs. 258nm)
Blank	7479	149	0
MCF7 fraction 56*	5401	3357	0
57*	6275	2024	0
58	7354	1112	0
59	7992	773	0
60	8311	163/453	0
61	8479	154/379	0
62	8124	129	0
U2OS fraction 56*	815	7015	0
57*	4366	3880	0
58	6363	1683	0
59	7562	1184	0
60	8066	813	0
61	8341	598	0
62	8349	159/381	0
HEK293 fraction 56*	6806	1758	0
57*	4698	3266	0
58	7243	1572	0
59	7712	1152	0
60	7983	949	0
61	7839	805	0
62	7616	595	0

B

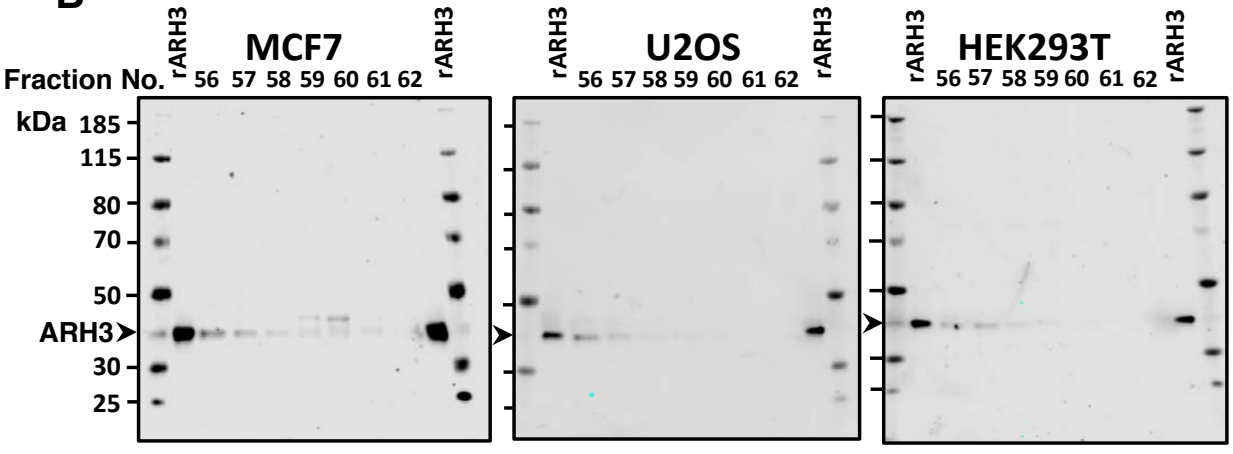

Figure S9. HPLC separation of α-NADase reaction products from the weak-anion exchange chromatography of U2OS, MCF7 and HEK293T cell lysates.

MCF7 (500μg), U20S (500ug), HEK293T (500μg) cell lysates were separated by HPLC weak-anion exchange chromatography as described in Methods. Fractions (180μL) were assayed for α-NADase activity overnight at 30°C, **A**. The absorbances at 258nm are reported. α-NAD and AMP were determined by the elution time of an α-NAD and AMP standard. **B**. Total volumes remaining of the fractions were analyzed for ARH3 immunoreactivity (*) see Methods.

Figure S10

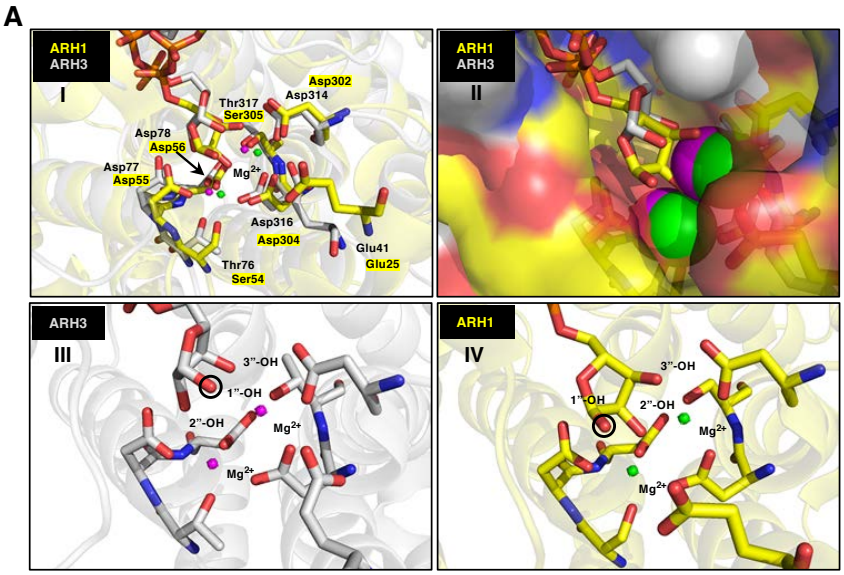

B

```
ARH3 (6D36) 37 GSFYEAHDTV 46-----73 LYYTDDTAMA 82-----313 GDTDTIATMA 322
ARH1 (6G28) 21 NGKWEFLQDG 30-----51 WRVSDDTVMH 60-----301 GDSDSTAAIA 310
```

Figure S10. Structure of the complex formed by human ARH1 and ARH3 binding to ADP-ribose and Mg^{2+} ions.

A. Crystal structure of ARH1 (yellow) and ARH3 (gray) with ADP-ribose and Mg^{2+} (ARH1-green and ARH3-magenta). Glu25, Ser54, Asp55, Asp56, Asp302, Asp304, and Ser305 in ARH1 (yellow highlight) and Glu41, Thr76, Asp77, Asp78, Asp314, Asp316, and Thr317 in ARH3 hydrogen-bonding residues near Mg^{2+} are critical for binding of ADP-ribose, and ARH1 and ARH3 hydrolase activities (e.g., ADP-ribosylarginine hydrolase, ADP-ribosylserine hydrolase, or poly-ADP-ribose)[1-4] **(I)**. Close-up surface representation of ARH1 and ARH3 with electro-negative and -positive atoms shown in red and blue. The binding pocket for ADP-ribose on surface of ARH1 and ARH3 is near the bound Mg^{2+} ions **(II)**. Close-up two Mg^{2+} ions and ADP-ribose binding in ARH3 **(III)** and ARH1 **(IV)**. The black circle in ARH1 and ARH3 indicates the 1”-OH of the distal ADP-ribose that is a site for cleavage[5]. Also, 1”-OH of the distal ADP-ribose in ARH1 and ARH3 has a negative influence on the binding of ADP-ribose[4] **(III) (IV)**. Crystal structures of the ARHs and macrodomains with bound ADP-ribose revealed a similar core-binding pocket.

B. Structure-guided alignment of selected ARHs protein sequence bound with Mg^{2+} ions. The selected residues (• red) in ARH1 and ARH3 contributed to the binding of ADP-ribose and Mg^{2+} ions as well as ADP-ribosylarginine, ADP-ribosylserine, or poly-ADP-ribose hydrolase catalytic activity.

Supporting References

1. Konczalik, P., and Moss, J. (1999) Identification of critical, conserved vicinal aspartate residues in mammalian and bacterial ADP-ribosylarginine hydrolases, *J Biol Chem 274*, 16736-16740.
2. Kato, J., Zhu, J., Liu, C., and Moss, J. (2007) Enhanced sensitivity to cholera toxin in ADP-ribosylarginine hydrolase-deficient mice, *Mol Cell Biol 27*, 5534-5543.
3. Moss, J., Jacobson, M. K., and Stanley, S. J. (1985) Reversibility of arginine-specific mono(ADP-ribosyl)ation: identification in erythrocytes of an ADP-ribose-L-arginine cleavage enzyme, *Proc Natl Acad Sci U S A 82*, 5603-5607.
4. Rack, J. G. M., Ariza, A., Drown, B. S., Henfrey, C., Bartlett, E., Shirai, T., Hergenrother, P. J., and Ahel, I. (2018) (ADP-ribosyl)hydrolases: Structural Basis for Differential Substrate Recognition and Inhibition, *Cell Chem Biol 25*, 1533-1546 e1512.
5. Pourfarjam, Y., Ventura, J., Kurinov, I., Cho, A., Moss, J., and Kim, I. K. (2018) Structure of human ADP-ribosyl-acceptor hydrolase 3 bound to ADP-ribose reveals a conformational switch that enables specific substrate recognition, *J Biol Chem 293*, 12350-12359.